Journal of Alloys and Compounds 514 (2012) 157–162

Contents lists available at SciVerse ScienceDirect

Journal of Alloys and Compounds

journal homepage: www.elsevier.com/locate/jallcom

Controlled synthesis and luminescence properties of $NaLnW_2O_8$ nanocrystals

Ying Li, Wei Zhou, Cheng Wang, Kai Pan, Naiying Fan, Guofeng Wang*, Chunmei Sun, Peng Mei

Key Laboratory of Functional Inorganic Material Chemistry, Ministry of Education, School of Chemistry and Materials Science, Heilongjiang University, Harbin 150080, People's Republic of China

ARTICLE INFO

Article history:
Received 13 October 2011
Received in revised form 6 November 2011
Accepted 9 November 2011
Available online 18 November 2011

Keywords:
$NaYW_2O_8$
Lanthanide ions
Nanocrystals
Optical properties

ABSTRACT

Tetragonal phase $NaLnW_2O_8$ (Ln = Y, Yb, Er, Tm, Eu, Gd, Ho, Ce, and Sm) nanocrystals were successfully prepared via a hydrothermal method. It is found that large ionic radii of lanthanide ions and high reaction temperature are beneficial for the formation of $NaLnW_2O_8$. The upconversion luminescence properties of $NaYW_2O_8$:Yb^{3+}/Er^{3+} and $NaYW_2O_8$:Yb^{3+}/Tm^{3+} were studied under 980 nm excitation. It is found that the luminescence intensity of $^2H_{11/2} \rightarrow {}^4I_{15/2}$ is much stronger than that of $^4S_{3/2} \rightarrow {}^4I_{15/2}$ as well as $^4F_{9/2} \rightarrow {}^4I_{15/2}$ in $NaYW_2O_8$:Yb^{3+}/Er^{3+}. Interestingly, there is no apparent change in the intensity ratio of $^2H_{11/2}/{}^4S_{3/2} \rightarrow {}^4I_{15/2}$ to $^4F_{9/2} \rightarrow {}^4I_{15/2}$ on Er^{3+} concentration. By analyzing the Raman spectrum, we suggested that the nonradiative relaxation of $^2H_{11/2} \rightarrow {}^4S_{3/2}$ is inefficient in $NaYW_2O_8$:Yb^{3+}/Er^{3+}, resulting in the strong $^2H_{11/2} \rightarrow {}^4I_{15/2}$ emission. The CIE coordinates of the green luminescence changed with excitation power. While for $NaYW_2O_8$:Yb^{3+}/Tm^{3+}, the CIE coordinates of the blue luminescence (0.14, 0.10) is almost unchanged with excitation power. In addition, the photoluminescence of $NaYW_2O_8$:Eu^{3+} excited at different wavelengths was studied in detail.

1. Introduction

Lanthanide-doped crystalline and amorphous materials have become a specific topic of interest owing to their unique luminescence prosperities [1–3]. Compared with conventional luminescent materials, such as organic fluorescent dyes and semiconductor quantum dots, lanthanide-doped materials can present low photobleaching, narrow emission bands, and longer luminescent lifetimes [4–6]. Recently, there has been increasing interest in the doping of nanocrystalline hosts with ions of the lanthanide elements because phosphors in the nanoscales can exhibit novel capabilities, depending on their structure, shape and size, such as tunable wavelengths [6], high efficiencies [7], and rapid responsibilities [8]. So far, the luminescent nanocrystals are considered as potentially useful active components in new optoelectronic devices and luminescent labels for biomolecules [9–11].

Double alkaline lanthanide molybdates and tungstates ABM_2O_8 (A: K^+, Na^+; B: trivalent lanthanide; M: W^{6+}, Mo^{6+}), which share a scheelite-like isostructure, show excellent thermal and hydrolytic stability and are considered to be efficient luminescent host materials [12–19]. Especially, the concentration quenching effect hardly occurs in ABM_2O_8 doped with lanthanide ions [20]. For a long period, the investigations on the ABM_2O_8 compounds have been focused on the single crystals as solid-state laser hosts and their optoelectronics applications [12–19]. In recent years, the controllable synthesis and luminescence properties of lanthanide-doped ABM_2O_8 micro/nanocrystals have also attracted increasing attention [21–26]. For example, Fan et al. synthesized $NaY(WO_4)_2$:Eu^{2+} and $NaY(WO_4)_2$:Yb^{3+}/Er^{3+} nanoparticles by a hydrothermal method and investigated their optical properties [24]. Kasuya and Isobe synthesized $NaEuW_2O_8$ nanophosphors and Zhou et al. reported flower-like $NaY(MoO_4)_2$:Eu^{3+} microarchitectures [25,26]. However, there have been no reports on $NaY(WO_4)_2$:Yb^{3+}/Tm^{3+} nanocrystals to date.

Here, tetragonal phase $NaLnW_2O_8$:Ln^{3+} (Ln = Y, Yb, Er, Tm, Eu, Gd, Ho, Ce, and Sm) nanocrystals were synthesized by a hydrothermal method. The results indicated that the formation of tetragonal $NaLnW_2O_8$ is closely related to the lanthanide ionic radius. The larger ionic radius is beneficial for the formation of $NaLnW_2O_8$. The optical properties of $NaYW_2O_8$ nanocrystals doped with different lanthanide ions were studied in detail.

2. Experimental

2.1. Synthesis

Analytical grade $Ln(NO_3)_3{\cdot}6H_2O$ (Ln = Y, Yb, Er, Tm, Eu, Gd, Ho, Ce, and Sm) (99.99%), NaF, ethanol, and oleic acid were obtained from Beijing Chemical Reagents, China. All of the reagents and solvents were used as received without further purification. Deionized water was used throughout.

Synthesis of $NaLnW_2O_8$ nanocrystals: in a typical synthesis, 1 mL of Na_2WO_4 aqueous solution (0.5 mol/L) and 1 mL of $Ln(NO_3)_3$ aqueous solution (0.5 mol/L) were added to a mixture of NaOH (1.2 g), ethanol (8 mL), deionized water (4 mL), and oleic acid (20 mL), and the solution was thoroughly stirred. Subsequently, the milky colloidal solution was transferred to a 50 mL Teflon-lined autoclave, and heated at

* Corresponding author. Tel.: +86 451 89359680; fax: +86 451 89359680.
E-mail address: wanggf75@gmail.com (G. Wang).

0925-8388/$ – see front matter © 2011 Elsevier B.V. All rights reserved.
doi:10.1016/j.jallcom.2011.11.046

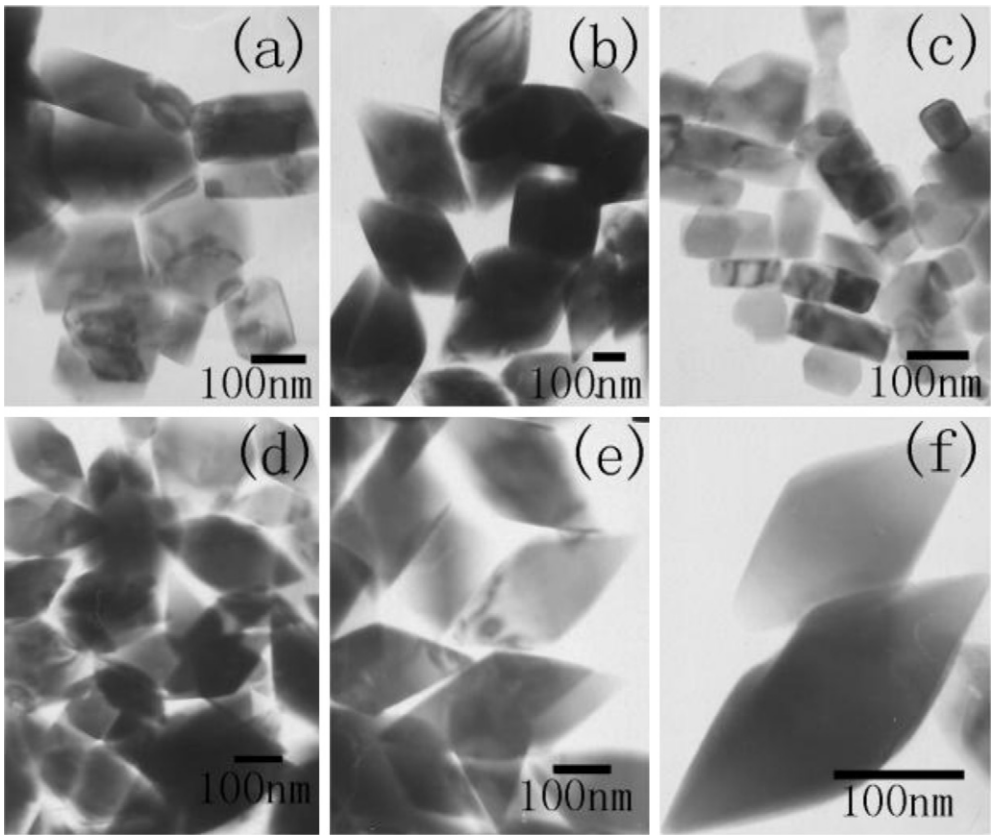

Fig. 1. TEM images of $NaYW_2O_8$ (a), $NaYbW_2O_8$ (b), $NaErW_2O_8$ (c), $NaTmW_2O_8$ (d, e), and $NaEuW_2O_8$ (f) prepared at 180 °C (1 ml of $Ln(NO_3)_3$ aqueous solution and 1 mL of Na_2WO_4 aqueous solution as raw materials).

160–180 °C for 24 h. The systems were then allowed to cool to room temperature. The final products were collected by means of centrifugation, washed with ethanol, and finally dried in vacuum at 80 °C for 4 h.

Synthesis of $NaYF_4:Yb^{3+}/Er^{3+}$ nanocrystals (see Refs. [27–29]): 0.5 mmol of $Ln(NO_3)_3$ aqueous solution and 4 mL of sodium fluoride solution (0.5 mol/L) were added to a mixture of NaOH (1.2 g), ethanol (8 mL), deionized water (8 mL), and oleic acid (20 mL), and the solution was thoroughly stirred. Subsequently, the milky colloidal solution was transferred to a 50 mL Teflon-lined autoclave, and heated at 180 °C for 24 h. The systems were then allowed to cool to room temperature. The final products were collected by means of centrifugation, washed with ethanol, and finally dried in vacuum at 80 °C for 4 h.

2.2. Characterization

The powder diffraction patterns were analyzed by a Rigaku (Japan) D/MAX-rA X-ray diffractionmeter (XRD) equipped with graphite monochromatized Cu Kα radiation (γ = 1.541874 Å), keeping the operating voltage and current at 40 kV and 40 mA, respectively. The size and morphology of the final products were observed by using the JEOL-2010 transmission electron microscope (TEM). Samples were prepared by placing a drop of a dilute cyclohexane dispersion of the nanocrystals on the surface of a copper grid. The down-conversion luminescence spectra were recorded with a Hitachi F-4500 fluorescence spectrophotometer at room temperature. For comparison of the luminescence properties of different samples, the luminescence spectra were measured with the same instrument parameters (2.5 nm for spectral resolution (FWHM) of the spectrophotometer and 400 V for PMT voltage) at room temperature. The up-conversion luminescence spectra were recorded by using the spectrophotometer with an adjustable laser (980 nm, Beijing Hi-Tech Optoelectronic Co., China) as the excitation source with a fiber-optic accessory. Raman spectra were taken by using Renishaw 1000 Micro-Raman spectrometer.

3. Results and discussion

3.1. Crystal structure and morphology

Figure S1(a–e) in the Supporting Information shows the XRD patterns of $NaLnW_2O_8$ (Ln = Y, Yb, Tm, Er, and Eu) with 1 ml of $Ln(NO_3)_3$ aqueous solution and 1 mL of Na_2WO_4 aqueous solution as raw materials prepared at 180 °C for 24 h. These patterns are in agreement with the tetragonal $NaYW_2O_8$ (JCPDS 48-0886), $NaYbW_2O_8$ (25-0887), $NaErW_2O_8$, $NaTmW_2O_8$, and $NaEuW_2O_8$, respectively. No other impurity peaks were detected. In addition, the peaks of $NaEuW_2O_8$ shift a little to the small diffraction angle in comparison with those of $NaYW_2O_8$, $NaYbW_2O_8$, $NaTmW_2O_8$, and $NaErW_2O_8$. It is imperative to point out that the XRD patterns of $NaErW_2O_8$, $NaTmW_2O_8$, and $NaEuW_2O_8$ could not be found in the JCPDS database. Figure S1(f, g) in the Supporting Information shows the XRD patterns of $NaYW_2O_8:Eu^{3+}$ and $NaYW_2O_8:Yb^{3+}/Er^{3+}$, which are similar to that of $NaYW_2O_8$. The corresponding TEM images of the as-prepared nanocrystals are shown in Fig. 1. The shape of $NaYW_2O_8$ and $NaErW_2O_8$ nanocrystals is almost rectangular, while those of $NaYbW_2O_8$, $NaTmW_2O_8$, and $NaEuW_2O_8$ are rhombic.

When the reaction temperature is 160 °C, only tetragonal $NaEuW_2O_8$ nanocrystals can be synthesized, as shown in Figure S2(f) in the Supporting Information. The other patterns in Figure S2(a–e) in the Supporting Information could not be found in the JCPDS database. We suggest that the formation of tetragonal $NaLnW_2O_8$ must be closely related to the lanthanide ionic radius, and larger ionic radius is beneficial for the formation of $NaLnW_2O_8$. To prove the correctness of the judgment, we have synthesized several samples with larger lanthanide ionic radius under the same reaction conditions, such as Gd^{3+}, Ho^{3+}, Ce^{3+}, and Sm^{3+}. As expected, tetragonal $NaGdW_2O_8$, $NaHoW_2O_8$, $NaEuW_2O_8$, $NaCeW_2O_8$, and $NaSmW_2O_8$ were successfully prepared when the reaction temperature is 160 °C (Figure S3 in the Supporting Information). We also studied the products with 2 mL of $Ln(NO_3)_3$ aqueous solution and 2 mL of Na_2WO_4 aqueous solution as raw materials prepared at 160 °C, as shown in Figure S4 in the Supporting Information. In comparison with the XRD patterns in

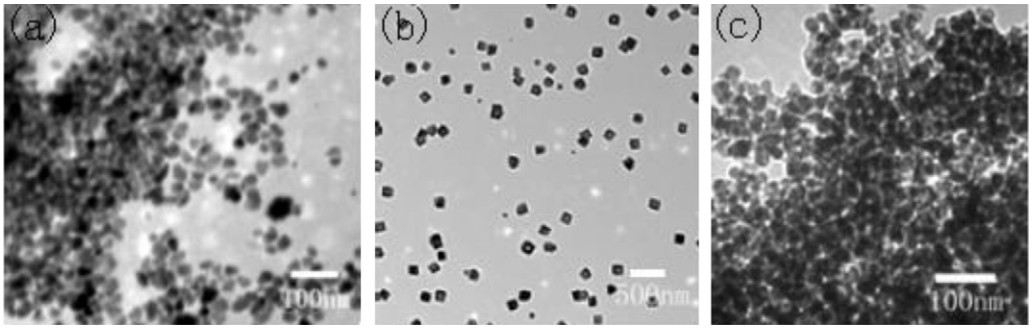

Fig. 2. TEM images of the samples with different Na_2WO_4 contents as raw materials prepared at 160 °C (the $Y(NO_3)_3$ content is 2 mL): (a) 2 mL, (b) 1 mL, and (c) 0.5 mL.

Figure S2 in the Supporting Information, no obvious change have been observed. Fig. 2 shows the TEM images of the samples with different Na_2WO_4 contents as raw materials prepared at 160 °C. Here, the $Y(NO_3)_3$ content is 2 mL. The nanoparticles observed from TEM images tended to aggregate.

3.2. Green UC luminescence of $NaYW_2O_8:Yb^{3+}/Er^{3+}$

Fig. 3a shows the UC luminescence spectra of the as-prepared $NaYW_2O_8:Yb^{3+}/Er^{3+}$ under different excitation powers. The spectral peaks correspond to the following transitions: $^4F_{7/2} \rightarrow {}^4I_{15/2}$ (~490 nm), $^2H_{11/2} \rightarrow {}^4I_{15/2}$ (~521 nm), $^4S_{3/2} \rightarrow {}^4I_{15/2}$ (~543 nm), and $^4F_{9/2} \rightarrow {}^4I_{15/2}$ (~653 nm). It is surprising to observe that the $^2H_{11/2} \rightarrow {}^4I_{15/2}$ emission of $NaYW_2O_8:Yb^{3+}/Er^{3+}$ is always the strongest, which is different from that of $NaYF_4:Yb^{3+}/Er^{3+}$, as shown in Fig. 3b. For $NaYF_4:Yb^{3+}/Er^{3+}$, the $^4S_{3/2} \rightarrow {}^4I_{15/2}$ emission is the strongest at low laser power and the $^2H_{11/2} \rightarrow {}^4I_{15/2}$ emission is the strongest at high laser power. It is known that the emission intensities and ratios of the various emissions are influenced by the doping levels, excitation power, and preparation temperature. Here, there is no apparent change in the intensity ratio of $^2H_{11/2} \rightarrow {}^4I_{15/2}$ to $^4S_{3/2} \rightarrow {}^4I_{15/2}$ on Er^{3+} concentration and preparation temperature. We suggest that the nonradiative relaxation of $^2H_{11/2} \rightarrow {}^4S_{3/2}$ in $NaYF_4:Yb^{3+}/Er^{3+}$ is more efficient than that in $NaYW_2O_8:Yb^{3+}/Er^{3+}$. Since the nonradiative relaxation is closely related to the phonon energies of the hosts, the Raman spectra of the $NaYW_2O_8$ and $NaYF_4$ were studied, as shown in Fig. 4. For the $NaYW_2O_8$, six Raman bands centered at ~132.6, 203.2, 332.8, 401.6, 814.7, and 916.7 cm^{-1} were observed. While for the $NaYF_4$, six Raman bands centered at ~146.7, 266.5, 396.1, 518.9, 639.8, and 797.9 cm^{-1} can be observed. The peaks at ~146.7, 266.5, 396.1, and 518.9 cm^{-1} of $NaYF_4$ are similar to those of the $NaYF_4:Yb^{3+}/Er^{3+}$ reported by Güdel and co-workers [30]. For the peaks at ~639.8 and 797.9 cm^{-1}, it is noted that the $NaYF_4$ was coated by oleic acid. And thus, the two peaks could be attributed to the vibrations from the organic surfactants. Similar results have also been reported by Shan et al. [31]. The energy separation between $^2H_{11/2}$ and $^4S_{3/2}$ levels of Er^{3+} ions in $NaYF_4:Yb^{3+}/Er^{3+}$ is about 518 cm^{-1} [32]. One phonon with ~518.9 cm^{-1} or two phonons with 266.5 cm^{-1} in $NaYF_4:Yb^{3+}/Er^{3+}$ can match the energy separation between $^2H_{11/2}$ and $^4S_{3/2}$, resulting in the effectively nonradiative relaxation of $^2H_{11/2} \rightarrow {}^4S_{3/2}$ in $NaYF_4:Yb^{3+}/Er^{3+}$. Consequently, the nonradiative relaxation of $^2H_{11/2} \rightarrow {}^4S_{3/2}$ in $NaYF_4:Yb^{3+}/Er^{3+}$ is more efficient than that in $NaYW_2O_8:Yb^{3+}/Er^{3+}$. It is noted that there is little shift in the position of the green emissions between $NaYF_4:Yb^{3+}/Er^{3+}$ and $NaYW_2O_8:Yb^{3+}/Er^{3+}$.

Fig. 5 shows the normalized UC luminescence spectra of $NaYW_2O_8:Yb^{3+}/Er^{3+}$ with different Er^{3+} concentrations. From the bottom to the top in Fig. 5, the concentrations of Er^{3+} ions are 5%, 10%, 30%, and 70%, respectively. There is no apparent change in the intensity ratio of $^2H_{11/2}/{}^4S_{3/2} \rightarrow {}^4I_{15/2}$ to $^4F_{9/2} \rightarrow {}^4I_{15/2}$ on Er^{3+} concentration, which is also different from that of $NaYF_4:Yb^{3+}/Er^{3+}$ reported previously [32]. For $NaYF_4:Yb^{3+}/Er^{3+}$, when the Er^{3+} concentration is high enough (70%), the $^4F_{9/2} \rightarrow {}^4I_{15/2}$ emission is the strongest [32]. In addition, the emission intensities increased with Er^{3+}/Yb^{3+} concentration and preparation temperature. The concentration quenching effect was not observed.

The CIE chromaticity coordinates were calculated from the UC luminescence spectra of $NaYW_2O_8:Yb^{3+}/Er^{3+}$ (10%) under different excitation powers, as shown in Table 1. The CIE coordinates of

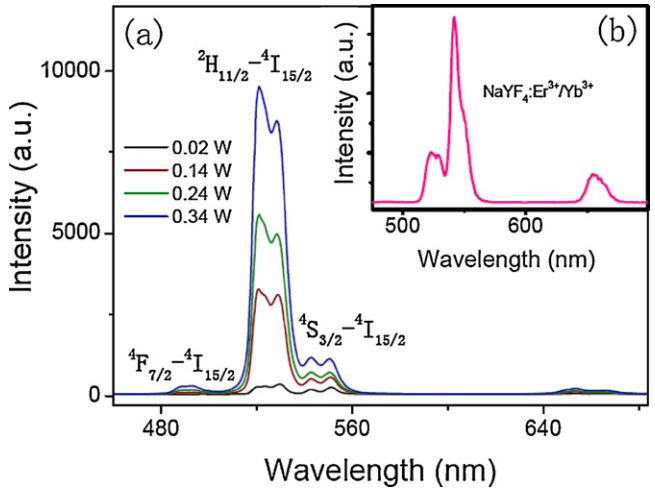

Fig. 3. UC luminescence spectra of (a) $NaYW_2O_8:Yb^{3+}/Er^{3+}$ and (b) $NaYF_4:Yb^{3+}/Er^{3+}$ excited with a 980 nm laser.

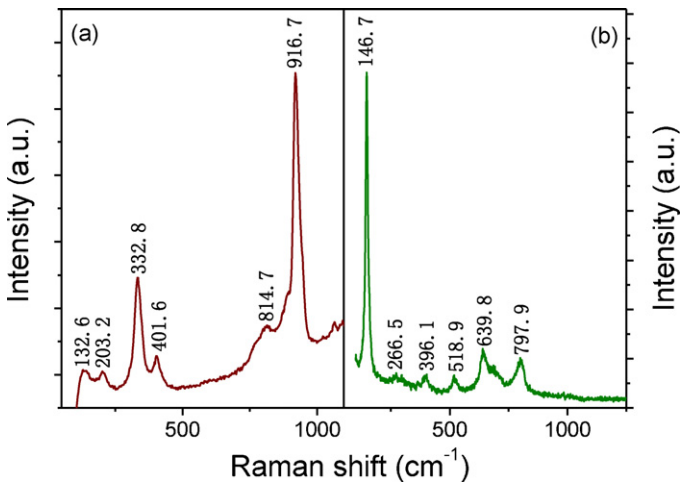

Fig. 4. Raman spectra of (a) $NaYW_2O_8$ and (b) $NaYF_4$ (the laser excitation wavelength was 633 nm).

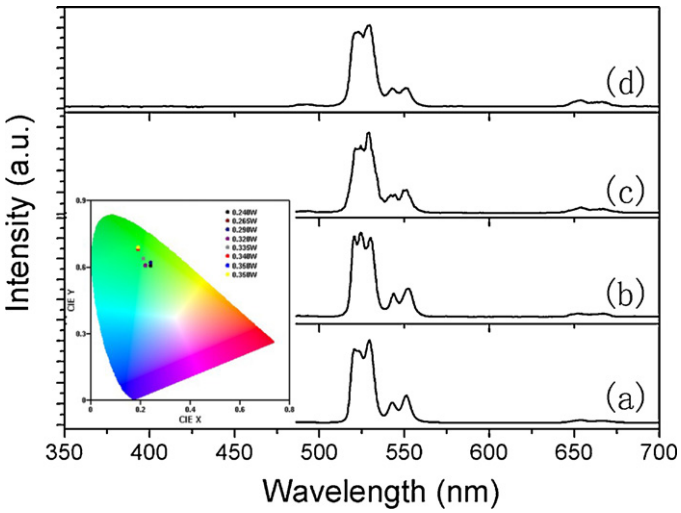

Fig. 5. Dependence of UC luminescence spectra (normalized to $^2H_{11/2} \rightarrow {}^4I_{15/2}$ transition) of $NaYW_2O_8$:Yb^{3+}/Er^{3+} on Er^{3+} concentration (20% Yb^{3+}): (a) 5%, (b) 10%, (c) 30%, and (d) 70%. Inset shows the CIE 1931 chromaticity diagram of $NaYW_2O_8$:Yb^{3+}/Er^{3+}(10%) under different excitation powers.

Table 1
The CIE chromaticity coordinates calculated from UC luminescence spectra of $NaYW_2O_8$:Yb^{3+}/Er^{3+} and $NaYW_2O_8$:Yb^{3+}/Tm^{3+} under different excitation powers.

Excitation power	CIE (*x*, *y*) of Er^{3+}	CIE (*x*, *y*) of Tm^{3+}
0.240 W	(0.24, 0.61)	(0.14, 0.11)
0.265 W	(0.24, 0.62)	(0.14, 0.10)
0.290 W	(0.24, 0.62)	(0.14, 0.10)
0.320 W	(0.22, 0.61)	(0.14, 0.10)
0.335 W	(0.21, 0.64)	(0.14, 0.10)
0.340 W	(0.19, 0.68)	(0.14, 0.10)
0.350 W	(0.19, 0.69)	(0.14, 0.10)
0.365 W	(0.18, 0.72)	(0.14, 0.10)

the green luminescence were (0.24, 0.61), (0.24, 0.62), (0.24, 0.62), (0.22, 0.61), (0.21, 0.64), (0.19, 0.68), (0.19, 0.69), and (0.18, 0.72) for 0.240, 0.265, 0.290, 0.320, 0.335, 0.340, 0.335, 0.340, 0.350, and 0.365 W, respectively. Obviously, the CIE coordinate of the green luminescence changed with excitation power. The intensity ratio of $^2H_{11/2}/{}^4S_{3/2} \rightarrow {}^4I_{15/2}$ to $^4F_{9/2} \rightarrow {}^4I_{15/2}$ as well as $^2H_{11/2} \rightarrow {}^4I_{15/2}$ to $^4S_{3/2} \rightarrow {}^4I_{15/2}$ increased with excitation power.

For an unsaturated UC process, the emission intensity (I_f) will be proportional to some power (n) of the infrared excitation (P) power:

$$I_f \propto P^n \quad (1)$$

where n is the number of infrared photons absorbed per visible photon emitted [33]. To investigate the fundamental UC mechanisms of $NaYW_2O_8$:Yb^{3+} (20%)/Er^{3+} (5%), the pumping power dependence of the fluorescent radiations was investigated. Fig. 6 shows the double logarithmic plots of the emission intensity as a function of excitation power for the $^4S_{3/2} \rightarrow {}^4I_{15/2}$, $^2H_{11/2} \rightarrow {}^4I_{15/2}$, and $^4F_{9/2} \rightarrow {}^4I_{15/2}$ emissions. The corresponding slopes (n) of the dependencies are listed in Table 2.

Table 2
Experimental slopes (n) of the dependencies log(emission intensity) versus log(excitation power) for $NaYW_2O_8$:Yb^{3+}/Er^{3+} and $NaYW_2O_8$:Yb^{3+}/Tm^{3+}.

Transition of Er^{3+}	n (Er^{3+})	Transition of Tm^{3+}	n (Tm^{3+})
$^2H_{11/2}/{}^4S_{3/2} \rightarrow {}^4I_{15/2}$	2.27	$^1D_2 \rightarrow {}^3H_6$	1.86
$^4F_{9/2} \rightarrow {}^4I_{15/2}$	0.95	$^1G_4 \rightarrow {}^3H_6$	2.50
–	–	$^3H_4 \rightarrow {}^3H_6$	1.78

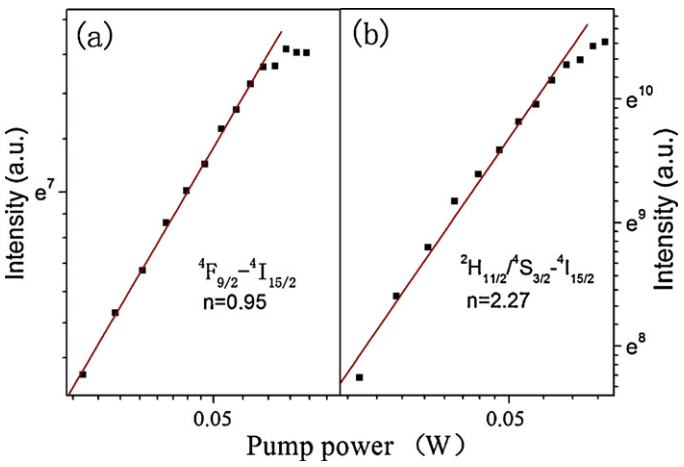

Fig. 6. Plots (log–log) of emission intensity versus pump power density: (a) $^4F_{9/2} \rightarrow {}^4I_{15/2}$ and (b) $^2H_{11/2}/{}^4S_{3/2} \rightarrow {}^4I_{15/2}$.

Although it is well known that the population of the $^4F_{9/2}$ comes from a two-photon process, the value of n for red emission ($^4F_{9/2} \rightarrow {}^4I_{15/2}$) was determined to be 0.95 in the $NaYW_2O_8$:Yb^{3+}/Er^{3+} (10%) nanocrystals. Pollnau et al. [34] attributed this phenomenon to the "saturation process" due to the competition between linear decay and UC processes for the depletion of the intermediate excited states [35]. According to their report, the value of n for a two-phonon process is ~2 when the linear decay of the intermediate state is dominant mechanism, while n is ~1 when the UC is the dominant in the Yb^{3+}/Er^{3+} codoped system. The intermediate level of the red emission is $^4I_{13/2}$, and therefore, the UC is the dominant depletion mechanism for $^4I_{13/2}$. In addition, the energy mismatch of Yb^{3+}–Er^{3+} energy transfer for re-excitation of the $^4I_{13/2}$ state is ~750–1400 cm^{-1} and the dominant phonon mode of $NaYW_2O_8$ is fund to be at ~916.7 cm^{-1}, and therefore, the second upward excitation from $^4I_{13/2}$ to $^4F_{9/2}$ in Er^{3+} is possible with the assistance of 1–2 phonon of $NaYW_2O_8$ host [34]. The value of n for green emission bands was determined to be 2.27. This is in agreement with the formerly reported behavior, where a three-photon process is involved in populating the $^2H_{11/2}/{}^4S_{3/2}$ levels [35]. The ions in the $^2H_{9/2}$ may nonradiatively relax to $^2H_{11/2}/{}^4S_{3/2}$ levels, which produce green emissions.

When the excitation power is higher than 0.1 W, the UC luminescence deviates from a linear relationship. Gudel et al. attributed the decrease of the slopes at higher laser powers to a change in the main depopulation mechanism of the excited states [36]. According to their reports, in the low-power limit, the population of the state (Er^{3+}) should occur through energy transfer from Yb^{3+}, and the depopulation should occur through relaxation to all lower-lying states of Er^{3+}. While in the high-power limit, the term related to upconversion to any other state (Er^{3+}) is dominant compared to the emission to the lower-lying states (Er^{3+}). The processes of infrared excitation and UC emission were drawn in the energy level diagrams of Er^{3+} and Yb^{3+} ions, as shown in Fig. 7.

3.3. Blue UC luminescence of $NaYW_2O_8$:Yb^{3+}/Tm^{3+}

Fig. 8 shows the UC luminescence spectra of the as-prepared $NaYW_2O_8$:Yb^{3+}/Tm^{3+} nanocrystals under different excitation powers. The spectral peaks correspond to the following transitions: $^1D_2 \rightarrow {}^3H_6$ (~363 nm), $^1D_2 \rightarrow {}^3F_4$ (~454 nm), $^1G_4 \rightarrow {}^3H_6$ (~475 nm), $^3F_3 \rightarrow {}^3H_6$ (~689 nm), and $^3H_4 \rightarrow {}^3H_6$ (~795 nm). It is found that the $^1G_4 \rightarrow {}^3H_6$ emission of $NaYW_2O_8$:Yb^{3+}/Tm^{3+} is always the strongest. The emission intensities increased with Tm^{3+}/Yb^{3+} concentration and preparation temperature. The

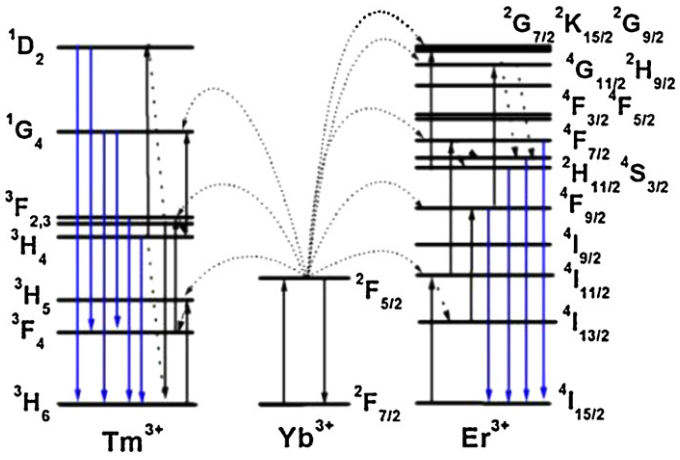

Fig. 7. Energy-level and UC schemes for the Yb^{3+}–Tm^{3+} and Yb^{3+}–Er^{3+} systems.

concentration quenching effect was not observed. The CIE chromaticity coordinates were calculated from UC luminescence spectra of $NaYW_2O_8$:Yb^{3+}/Tm^{3+} under different excitation powers, as shown in Table 1. There is no apparent change in the CIE coordinates (0.14, 0.10) of the blue luminescence.

Fig. 9 shows the double logarithmic plots of the emission intensity as a function of excitation power for the $^1D_2 \rightarrow {}^3H_6$, $^1G_4 \rightarrow {}^3H_6$, and $^3H_4 \rightarrow {}^3H_6$ emissions. The corresponding slopes (n) of the dependencies are listed in Table 2. The population of the states $^1D_2$, $^1G_4$, and $^3H_4$ ($^3F_3$) should come from four-photon, three-photon, and two-photon UC processes, respectively. The pump light excites only the Yb^{3+} ions, and three successive energy transfers from Yb^{3+} to Tm^{3+} populate $^3H_5$, $^3F_2$, and $^1G_4$ levels. The $^1D_2$ level of Tm^{3+} cannot be populated by the fourth photon from Yb^{3+} via energy transfer to the $^1G_4$ due to the large energy mismatch (about 3500 cm^{-1}) between them [32,34]. The cross-relaxation between Tm^{3+} ions may alternatively play an important role in populating $^1D_2$ level. The decrease of n for $^1D_2$ level is also attributed to the "saturation process" [37]. The processes of infrared excitation and UC emission were drawn in the energy level diagrams of Tm^{3+} and Yb^{3+} ions, as shown in Fig. 7. Similarly to that of $NaYW_2O_8$:Yb^{3+}/Er^{3+}, the UC luminescence deviates from a linear relationship in higher excitation power range, which can be attributed to a change in the main depopulation mechanism of the excited states [36].

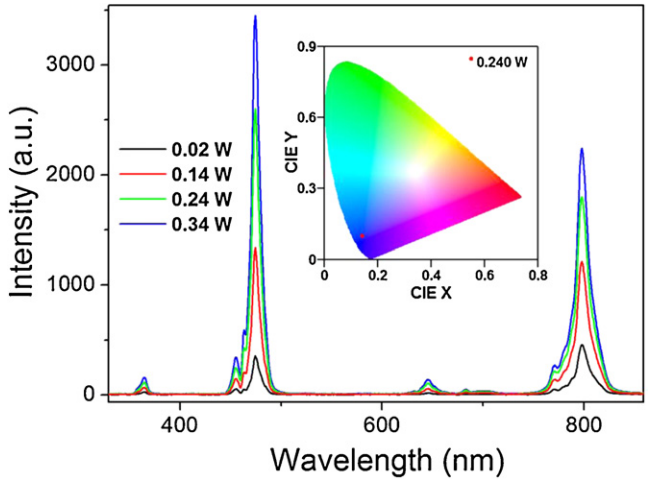

Fig. 8. UC luminescence spectra of $NaYW_2O_8$:Yb^{3+}/Tm^{3+} excited with a 980 nm laser. Inset shows the CIE 1931 chromaticity diagram of $NaYW_2O_8$:Yb^{3+}/Tm^{3+}.

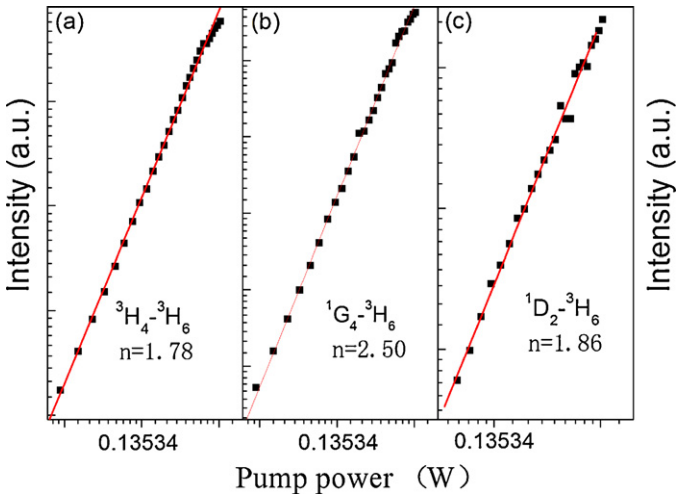

Fig. 9. Plots (log–log) of emission intensity versus pump power density: (a) $^3H_4 \rightarrow {}^3H_6$, (b) $^1G_4 \rightarrow {}^3H_6$, and (c) $^1D_2 \rightarrow {}^3H_6$.

3.4. Photoluminescence of $NaYW_2O_8$:Eu^{3+}

Fig. 10a shows the room-temperature excitation spectra of $NaYW_2O_8$:Eu^{3+} nanocrystals (monitored at 589, 613, 651, and 700 nm). The positions of these excitation peaks are practically identical to the characteristic absorption bands for f–f intra-configuration transitions in trivalent europium[38,39]. The most intense peak is centered at 465 nm. Fig. 10b shows the room-temperature emission spectra of $NaYW_2O_8$:Eu^{3+} nanocrystals under 394, 465, and 534 nm excitation. It can be observed that the emission intensities were the strongest when the excitation was performed at 465 nm. The $^5D_0 \rightarrow {}^7F_J$ (J = 1, 2, 3, and 4) transitions were observed. The $^5D_0 \rightarrow {}^7F_1$ transition is magnetic-dipole-allowed and its intensity is almost independent on the local environment around Eu^{3+} ions. The $^5D_0 \rightarrow {}^7F_2$ transition is electric-dipole-allowed due to an admixture of opposite parity $4f^{n-1}5d$ states by an odd parity crystal-field component. Therefore, its intensity is sensitive to the local structure around Eu^{3+} ions. The $^5D_0 \rightarrow {}^7F_3$ transition exhibits a mixed magnetic dipole and electric dipole character. The $^5D_0 \rightarrow {}^7F_4$ is electric dipole transition. It is well known that the intensity ratio of $^5D_0 \rightarrow {}^7F_2$ to $^5D_0 \rightarrow {}^7F_1$ is strongly dependent on the local symmetry of the Eu^{3+} ions. Therefore, Eu^{3+} ions are often used as probes to detect local environments

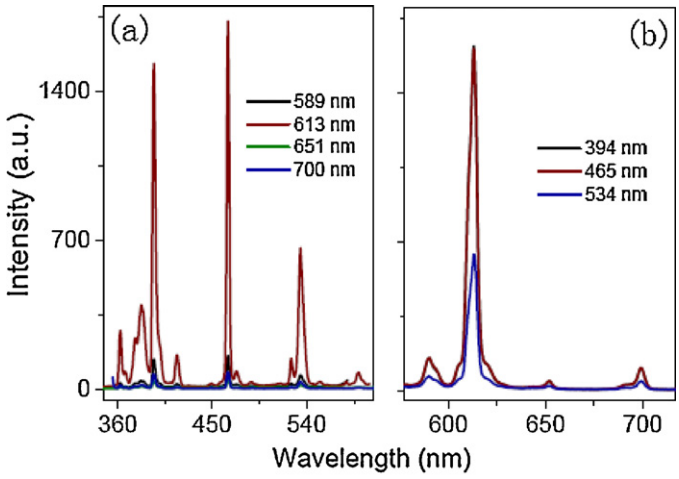

Fig. 10. Excitation (a) and emission (b) spectra of $NaYW_2O_8$:Eu^{3+} nanocrystals.

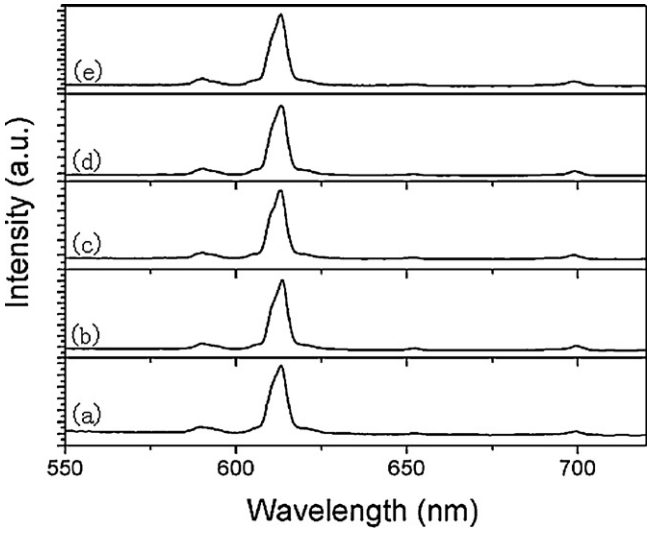

Fig. 11. Emission spectra of $NaYW_2O_8$:Eu^{3+} nanocrystals with different Eu^{3+} concentrations: (a) 1%, (b) 5%, (c) 10%, (d) 20%, and (e) 30%.

in a matrix. In a site with inversion symmetry the $^5D_0 \rightarrow {}^7F_1$ is dominating, while in a site without inversion symmetry the $^5D_0 \rightarrow {}^7F_2$ is the strongest. In the emission spectra of $NaYW_2O_8$:Eu^{3+} nanocrystals, the $^5D_0 \rightarrow {}^7F_2$ is much stronger than the $^5D_0 \rightarrow {}^7F_1$ [36,37]. Fig. 11 presents the emission spectra of $NaYW_2O_8$:Eu^{3+} nanocrystals with different Eu^{3+} concentrations. The peak positions and the shape of emissions were not influenced by Eu^{3+} concentration. The dependence of the intensity ratio of ($^5D_0 \rightarrow {}^7F_2$) to ($^5D_0 \rightarrow {}^7F_1$) on Eu^{3+} concentration indicates that there are no any apparent change in the local symmetry around Eu^{3+} ions with increasing Eu^{3+} concentration. The concentration quenching effect hardly occurs.

4. Conclusion

In this study, $NaLnW_2O_8$ nanocrystals were synthesized by a hydrothermal method. The nanocrystals can be produced in a simple procedure with high yields, and the optical properties of $NaYW_2O_8$ nanocrystals doped with different lanthanide ions were studied in detail. For the UC luminescence spectra of $NaYW_2O_8$:Yb^{3+}/Er^{3+} with different excitation powers, it is found that the $^2H_{11/2} \rightarrow {}^4I_{15/2}$ emission of $NaYW_2O_8$:Yb^{3+}/Er^{3+} is always the strongest, which is different from that of $NaYF_4$:Yb^{3+}/Er^{3+}. Especially, there is no apparent change in the intensity ratio of $^2H_{11/2}/{}^4S_{3/2} \rightarrow {}^4I_{15/2}$ to $^4F_{9/2} \rightarrow {}^4I_{15/2}$ on Er^{3+} concentration. These phenomena are related to nonradiative relaxation of $^2H_{11/2} \rightarrow {}^4S_{3/2}$. The Raman spectra of the $NaYW_2O_8$:Yb^{3+}/Er^{3+} and $NaYF_4$:Yb^{3+}/Er^{3+} indicate that the nonradiative relaxation of $^2H_{11/2} \rightarrow {}^4S_{3/2}$ in $NaYF_4$:Yb^{3+}/Er^{3+} is more efficient than that in $NaYW_2O_8$:Yb^{3+}/Er^{3+}. The CIE coordinate of the green luminescence changed with excitation power. For the UC luminescence spectrum of $NaYW_2O_8$:Yb^{3+}/Tm^{3+} nanocrystals, the CIE coordinate of the blue luminescence was (0.14, 0.10), which is almost unchanged with excitation power. For the $NaYW_2O_8$:Eu^{3+} nanocrystals, the $^5D_0 \rightarrow {}^7F_2$ is much stronger than the $^5D_0 \rightarrow {}^7F_1$. The emission intensities were the strongest when the excitation was performed at 465 nm. In addition, the concentration quenching effect was not observed.

Acknowledgements

This work was supported by the National Natural Science Foundation of China (10979032, 21171052, and 21101060), the Special Financial Grant from China Postdoctoral Science Foundation (201104456), the Natural Science Foundation of Heilongjiang Province (201118), and the Program for New Century Excellent Talents in University.

Appendix A. Supplementary data

Supplementary data associated with this article can be found, in the online version, at doi:10.1016/j.jallcom.2011.11.046.

References

[1] C.Y. Yan, A.J. Faber, H. Waal, P.G. Kik, A. Polman, Appl. Phys. Lett. 71 (1997) 2922–2924.
[2] A. Braud, S. Girard, J.L. Doualan, M. Tuau, R. Moncorge, A.M. Tkachuk, Phys. Rev.: Condens. Matter 61 (2000) 5280–5292.
[3] J. Huang, Y. Chen, X. Gong, Y. Lin, Z. Luo, Y. Huang, J. Opt. Soc. Am. B 27 (2010) 2605–2611.
[4] L.Y. Wang, P. Li, Y.D. Li, Adv. Mater. 19 (2007) 3304–3307.
[5] S. Sivakumar, P.R. Diamente, F. van Veggel, Chem. Eur. J. 12 (2006) 5878–5884.
[6] X. Bai, H.W. Song, G.H. Pan, Y.Q. Lei, T. Wang, X.G. Ren, S.Z. Lu, B. Dong, Q.L. Dai, L.B. Fan, J. Phys. Chem. C 111 (2007) 13611–13617.
[7] R.N. Bhargava, D. Gallaghar, X. Hong, A. Nurmikko, Phys. Rev. Lett. 72 (1994) 416419.
[8] Y.J. Kim, Y.S. Yang, S.C. Ha, S.M. Cho, Y.S. Kim, H.Y. Kim, H. Yang, Y.T. Kim, Sens. Actuators B 106 (2005) 189–198.
[9] K. Riwotzki, H. Meyssamy, H. Schnablegger, A. Komowski, M. Haase, Angew. Chem. Int. Ed. 40 (2001) 573–576.
[10] L.Y. Wang, R.X. Yan, Z.Y. Huo, L. Wang, J.H. Zeng, J. Bao, X. Wang, Q. Peng, Y.D. Li, Angew. Chem. Int. Ed. 44 (2005) 6054–6057.
[11] O. Lehmann, H. Meyssamy, K. Kolmpe, H. Schnablegger, M. Haase, J. Phys. Chem. B 107 (2003) 7449–7453.
[12] A. Lagatsky, X. Han, M. Serrano, C. Cascales, C. Zaldo, S. Calvez, M. Dawson, J. Gupta, C. Brown, W. Sibbett, Opt. Lett. 35 (2010) 3027–3029.
[13] F. Yang, F. Yan, Z. You, C. Tu, C. Sun, Y. Wang, Z. Zhu, J. Li, Laser Phys. Lett. 7 (2010) 867–869.
[14] L. Chen, S. Zhao, J. Zheng, Z. Cheng, C. Chen, Opt. Laser Technol. 34 (2002) 347–350.
[15] F. Yang, C. Sun, Z. You, C. Tu, G. Zhang, H. Zhu, Laser Phys. 20 (2010) 1695–1697.
[16] R. Lan, L. Pan, I. Utkin, Q. Ren, H. Zhang, Z. Wang, R. Fedosejevs, Opt. Express 18 (2010) 4000–4005.
[17] W. Zhou, X. Zhang, B. Chai, Adv. Solid State Lasers 10 (1997) 451–454.
[18] E. Rode, V. Karpov, M. Ivanova, Russ. J. Inorg. Chem. 16 (1971) 905–908.
[19] Z. Cheng, Q. Lu, S. Zhang, J. Liu, X. Yi, F. Song, Y. Kong, J. Han, H. Chen, J. Cryst. Growth 222 (2001) 797–800.
[20] X. Huang, G. Wang, J. Lumin. 130 (2010) 1702–1707.
[21] N. Xue, X. Fan, Z. Wang, M. Wang, Mater. Lett. 61 (2007) 1576–1579.
[22] B. Yan, J. Wu, Mater. Chem. Phys. 116 (2009) 67–71.
[23] K. Byrappa, A. Jain, J. Mater. Res. 11 (1996) 2869–2875.
[24] F. Wang, X. Fan, D. Pi, Z. Wang, M. Wang, J. Solid State Chem. 178 (2005) 825–830.
[25] R. Kasuya, T. Isobe, J. Electrochem. Soc. 156 (2009) J278–J282.
[26] Y. Huang, L. Zhou, L. Yang, Z. Tang, Opt. Mater. 33 (2011) 777–782.
[27] X. Wang, J. Zhuang, Q. Peng, Y.D. Li, Nature 437 (2005) 121–124.
[28] L.Y. Wang, Y.D. Li, Nano Lett. 6 (2006) 1645–1649.
[29] L.Y. Wang, Y.D. Li, Chem. Mater. 19 (2007) 727–734.
[30] C. Renero-Lecuna, R. Martín-Rodrígues, R. Valiente, J. González, F. Rodríguez, K. Krámer, H. Güdel, Chem. Mater. 23 (2011) 3442–3448.
[31] J. Shan, M. Uddi, N. Yao, Y. Ju, Adv. Funct. Mater. 20 (2010) 3530–3537.
[32] G.F. Wang, Q. Peng, Y.D. Li, Chem. Eur. J. 16 (2010) 4923–4931.
[33] M. Pollnau, D.R. Gamelin, S.R. Lüthi, H.U. Güdel, Phys. Rev. B 61 (2000) 3337–3346.
[34] G.F. Wang, Q. Peng, Y.D. Li, J. Am. Chem. Soc. 131 (2009) 14200–14201.
[35] Z. Cheng, S. Zhang, F. Song, H. Guo, J. Han, H. Chen, J. Phys. Chem. Solids 63 (2002) 2011–2017.
[36] J. Suyver, A. Aebischer, S. García-Revilla, P. Gerner, H. Güdel, Phys. Rev. B 71 (2005) 125123/1–125123/9.
[37] G.F. Wang, W.P. Qin, L.L. Wang, G.D. Wei, P.F. Zhu, R. Kim, Opt. Express 16 (2008) 11907–11914.
[38] G.F. Wang, Y. Li, B.J. Jiang, K. Pang, N.Y. Fan, Q.M. Feng, Y.J. Chen, C.G. Tian, Chem. Commun. 47 (2011) 8019–8021.
[39] G.F. Wang, W.P. Qin, D.S. Zhang, L.L. Wang, G.D. Wei, P.F. Zhu, R. Kim, J. Phys. Chem. C 112 (2008) 17042–17045.